Feedback-Related Dynamics of Hierarchical Error Processing in Goal-Directed Action

Niko Kroflic, Tjasa Kunavar, Kevin De Pauw, and Jan Babič, *Member, IEEE*

***Abstract*— The performance monitoring system is essential for adaptive behavior and the development of brain-machine interfaces that utilize neural feedback signals. The posterior medial frontal cortex generates different error-related potentials (ErrP), including error-related negativity (ERN), N2, and feedback-related negativity (FRN), which encode specific aspects of performance evaluation. In this study, we reexamine the hierarchical framework of error processing by investigating how low-level execution error detection and correction influence high-level outcome evaluation as reflected in FRN dynamics. Furthermore, we examine whether neural signals associated with outcome errors maintain consistent or distinct feature representations under different experimental conditions of altered feedback availability. Using a visuomotor rotation task, we manipulated the availability of visual feedback in three blocks to examine how immediate sensory error detection and corrective actions interact with outcome processing. Participants (n = 16) performed reaching movements while experiencing unexpected cursor rotations ($\pm 20^\circ$ and $\pm 40^\circ$; 20% probability) that challenged their sensorimotor control and task success. EEG recordings revealed that the FRN showed valence sensitivity in Blocks 1 and 3, while Block 2 exhibited a surprise-driven response without outcome differentiation. In contrast, posterior negativity appeared only in Blocks 1 and 3, where participants could detect and correct movement errors. This posterior response emerged on trials requiring corrective movements, regardless of final outcome, and appears to be driven by the availability of sensory feedback and error correction rather than by outcome valence. Furthermore, we demonstrate robust classification between low-level and high-level error signals and their conditional outcome-related variations, providing a foundation for more informative feedback in adaptive neural interfaces.**

***Index Terms*— Error-related potentials, feedback-related negativity, performance monitoring.**

I. Introduction

THE performance monitoring system plays a crucial role in adaptive behavior by evaluating actions, detecting errors, and guiding corrective actions to optimize interactions with the environment [1], [2], [3]. A key neural signature of this monitoring process is the error-related potential (ErrP), a broad class of neural signals associated with cognitive control and performance monitoring. ErrPs can be recorded non-invasively via electroencephalography (EEG) or invasively using techniques such as electrocorticography, as well as from single microelectrodes or microelectrode arrays [4], [5]. These signals have proven particularly valuable in the design of adaptive brain-machine interfaces (BMIs). Within such systems, ErrPs function as implicit feedback that indicates deviations from intended actions, serving as effective reinforcement learning signals for artificial agents [6], [7], [8], [9]. A promising approach to improve agent learning is to increase feedback specificity by differentiating between various error types. Previous studies, for instance, have reliably classified low-level execution errors (deviations in action execution) from high-level outcome errors (failures to achieve a task goal) [4], [10].

These error processes are mediated by the posterior medial frontal cortex, which generates several ErrP components, including the ERN, N2, and FRN [2], [11]. Although these components share anatomical origins, they are typically studied in separate paradigms emphasizing either response execution or outcome evaluation. Among these components, the FRN is specifically involved in reward prediction error processing [12], encoding both valence and surprise information [1], [13], [14], distributed across time and space [15]. Both execution-phase monitoring and outcome-phase evaluation have been hypothesized to represent prediction error signals [2], [3], [16]. Early investigations examined how these behaviorally distinct error types might interact, proposing that execution errors engage different neural processes than outcome errors [17], [18]. However, subsequent research has revealed that although the FRN is typically associated with outcome errors, it is also modulated by execution and selection errors and influenced by known factors such as reward contingencies [19], [20]. A limitation of these latter studies

Received 25 June 2025; revised 9 December 2025 and 6 March 2026; accepted 8 April 2026. Date of publication 13 April 2026; date of current version 22 April 2026. Associate Editor: Yingchun Zhang. This work was supported in part by Slovenian Research Agency under Grant P2-0076 and in part by European Community Horizon Europe program through the Soft Wearable Assistive Garments for Human Empowerment (SWAG) Project under Contract 101120408. *(Corresponding author: Niko Kroflic.)*

Niko Kroflic and Tjasa Kunavar are with the Laboratory for Neuromechanics and Biorobotics, Department of Automatics, Biocybernetics, and Robotics, Jožef Stefan Institute, SI-1000 Ljubljana, Slovenia, and also with the Jožef Stefan International Postgraduate School, SI-1000 Ljubljana, Slovenia (e-mail: niko.kroflic@ijs.si; tjasa.kunavar@ijs.si).

Kevin De Pauw is with the Human Physiology and Sports Physiotherapy Research Group, Vrije Universiteit Brussel, B-1050 Brussels, Belgium, and also with Brussels Human Robotics Research Center, B-1050 Brussels, Belgium (e-mail: Kevin.De.Pauw@vub.be).

Jan Babič is with the Laboratory for Neuromechanics and Biorobotics, Department of Automatics, Biocybernetics, and Robotics, Jožef Stefan Institute, SI-1000 Ljubljana, Slovenia (e-mail: jan.babic@ijs.si).

Digital Object Identifier 10.1109/TNSRE.2026.3683510

© 2026 The Authors. This work is licensed under a Creative Commons Attribution 4.0 License.
For more information, see https://creativecommons.org/licenses/by/4.0/

is that they constrained online sensory feedback or corrective movements. For instance, Mushtaq et al. [19] hid the cursor during movement execution and delayed endpoint feedback by 1 second, while Torrecillos et al. [21] used a shooting task where participants made rapid reaching movements with no opportunity to correct their trajectory. These constraints limit our understanding of how ongoing sensory feedback and subsequent corrective actions contribute to resolving high-level errors.

To address this gap, we adapt an experimental paradigm from Izawa and Shadmehr [22], which demonstrated that different learning mechanisms are engaged based on feedback availability. This allows us to separate the effects of sensory information and subsequent error correction on feedback-related neural responses. Our study diverges from previous work on motor learning [20], [22], and Torrecillos et al. [21] by introducing unexpected errors of varying magnitudes, a method drawn from Milekovic et al. [4] and Spüler and Niethammer [10] to simulate false decoding in BMI, while still permitting corrective movements. Specifically, we have two main objectives: 1) to investigate how the detection and correction of low-level execution errors influence high-level error responses, and 2) to examine whether neural signals associated with outcome errors exhibit consistent or distinct feature representations across different feedback conditions. To achieve this, our experimental design systematically manipulates the availability of visual feedback, isolating the respective contributions of real-time sensory feedback and error correction to the resolution of high-level errors.

II. Methods

A. Subjects

Participants were recruited through email lists at local universities in Ljubljana, Slovenia, advertised as a computer game involving EEG monitoring and interaction with a robot. All participants received detailed information regarding the experimental procedure and objectives, and provided informed consent approved by the Slovenian National Medical Committee (No. 0120-185/2023/3). The sample size was determined based on a previous study [10], with additional participants planned to compensate for potential experimental noise. Initially, 18 individuals participated. Data from two participants (subjects 4 and 7) were excluded due to problematic recording sessions, resulting in a final analyzed sample of 16 participants. The final sample consisted of healthy, right-handed individuals (4 females; mean age 26 ± 3 years), with right-handedness confirmed via self-report. Participants were required to be between 20 and 40 years old, have normal or corrected-to-normal vision, and report no history of neurological or psychiatric disorders.

B. Experimental Setup and Procedure

1) Apparatus and Stimuli: Participants were seated approximately 5 cm from the table edge and 30 cm from a 21-inch horizontal display screen (1920×1080 resolution), with their view of their hand blocked by a barrier. They controlled a cursor (0.4 cm diameter) using a haptic robot handle. The screen displayed the cursor, a starting position (white circle, 0.4 cm diameter), and a target circle (0.7 cm diameter) located 10 cm away. A dashed semicircular arc, centered on the start and passing through the target, represented the required movement distance. The experimental setup is shown schematically in Fig. 1.

2) Task Paradigm: While visuomotor rotation (VMR) is a standard paradigm for studying sensorimotor adaptation [22], we used it to examine the immediate neural responses to error events. To achieve this and prevent adaptation, on 20% of experimental trials, the visual feedback of the cursor was pseudorandomly rotated. This approach has been shown to effectively maintain participants in a state of early learning where errors remain salient and elicit robust neural responses [23], [24]. Each trial began with the haptic robot guiding the participant's hand to the starting position. After a 300 ms delay, the target turned blue, signaling the participant to initiate a center-out reaching movement. A trial was complete once the cursor's center intersected any point along the 10-cm semicircular arc. The task included two trial types: *Normal Trials* (no rotation) and *Rotation Trials*.

3) Experimental Conditions and Manipulations: The design of the experiment was based on the work of Izawa and Shadmehr [22] to dissociate learning mechanisms based on feedback availability. Here, we used a within-subject design, where each participant completed three sequential blocks defined by their feedback condition. The first block provided continuous visual feedback of the cursor's path but no explicit outcome feedback. The second block omitted the cursor's path, providing only explicit success/failure feedback after the movement. The third block combined both, providing continuous visual feedback and explicit outcome feedback. In the *Rotation Trials*, the cursor's displayed position (x', y') was transformed relative to its actual position (x, y) by the rotation matrix (R) shown in (1), where θ represents the angle of rightward (positive) or leftward (negative) rotation, randomly set to $\pm 20°$ or $\pm 40°$.

$$\begin{bmatrix} x' \\ y' \end{bmatrix} = \begin{bmatrix} \cos\theta & -\sin\theta \\ \sin\theta & \cos\theta \end{bmatrix} \begin{bmatrix} x \\ y \end{bmatrix} \tag{1}$$

This discrepancy produced an execution error (a deviation from the intended path), which could in turn lead to an outcome error (missing the target). Each block began with 20 practice trials (*Normal Trials*) to familiarize the participant with the feedback condition. This was followed by 200 experimental trials per block, for a total of 660 trials across the experiment. All participants completed the blocks in a fixed order (Block 1, 2, then 3), with a 1-minute pause between blocks. The average recording time was 40 ± 3 minutes.

4) Participant Instructions: The participants were instructed that their primary objective was to hit as many targets as possible and were informed that the cursor might not always follow their actual hand movement. They were encouraged to complete movements within a soft time window of 400–800 ms to promote homogeneity. If a movement was outside this range, feedback indicating *too fast* or *too slow* was displayed 1 second after the primary task feedback to avoid interference. Any trial lasting longer than 1 second was excluded from the analysis. Across all participants ($n = 16$), on average $2.3\% \pm 2.6\%$ of trials were excluded (range: 0.0%–9.1%).

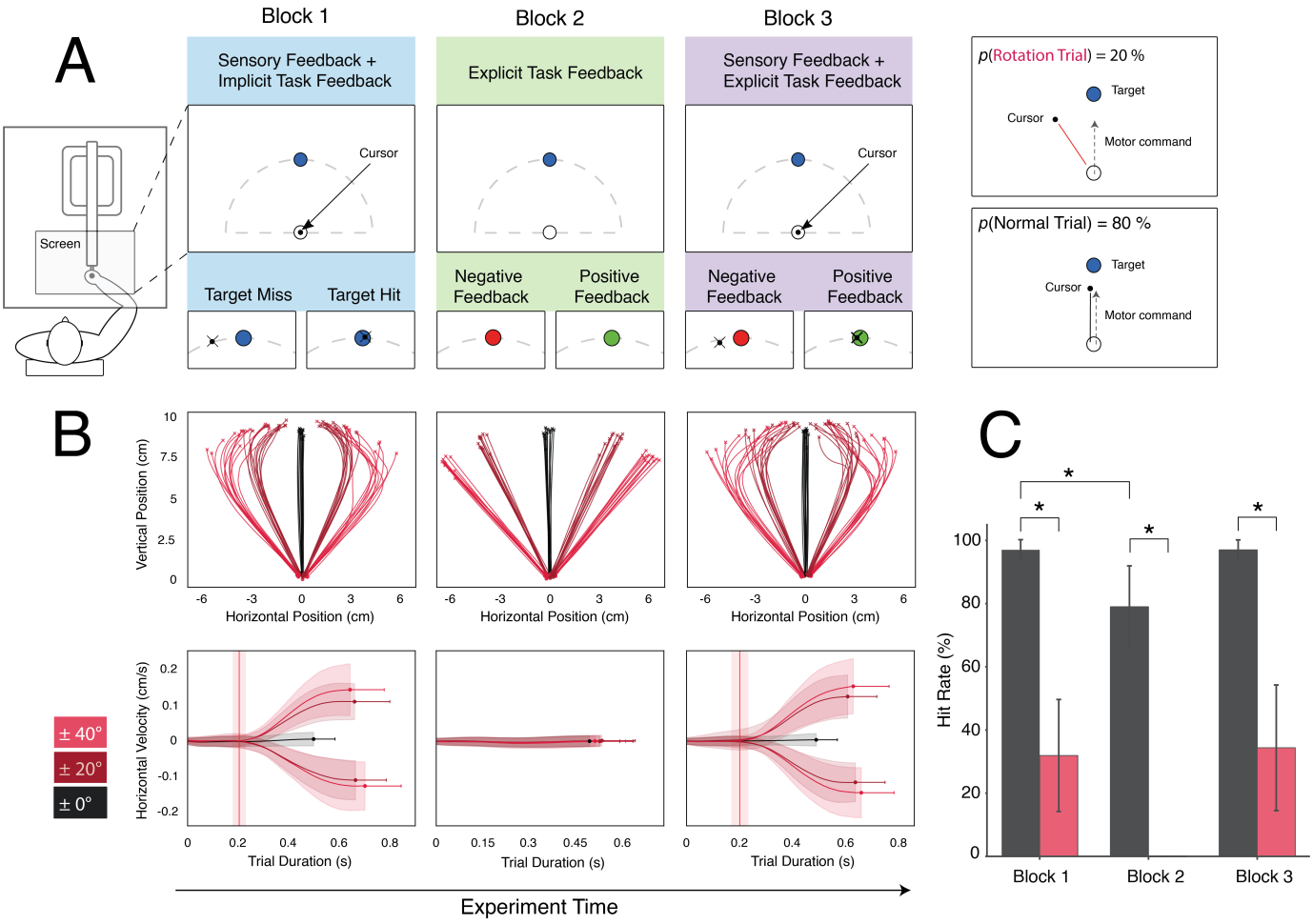

Fig. 1. **A)** Schematic of the experimental setup and task design. Left: A participant uses a haptic robot to control a cursor on a screen, with their hand view obstructed. Right: The three experimental blocks differed in visual feedback. Block 1 provided continuous cursor feedback. Block 2 removed cursor feedback but provided explicit outcome feedback (target changing to green for a hit or red for a miss). Block 3 provided both cursor and outcome feedback. **B)** Kinematic data across the three blocks. Top row: Mean cursor trajectories in the horizontal (x) and vertical (y) plane. Bottom row: Grand-average horizontal velocity (v_x) profiles. Shaded areas represent ± 1 standard deviation (SD) around the mean. The endpoint of each trace indicates the mean trial duration (± 1 SD, horizontal error bars). Vertical red lines denote the mean correction onset time. **C)** Mean hit rate for Normal (black) and Rotation (red) trials across blocks. Error bars represent the 95% confidence interval. Asterisks indicate a significant difference between trial types and blocks ($p < 0.05$).

C. EEG and Kinematic Data Acquisition

EEG activity was recorded using an *actiCHamp Plus 64 electrode EEG system* (BrainVision, Brain Products GmbH, Gilching, Germany) referenced to the POz channel. Electrodes were positioned following the international 10–20 system [25]. To monitor horizontal eye movements, two electrodes were placed at the outer canthi of the left and right eyes. Data were sampled at 500 Hz, and electrode impedances were maintained below 10 kΩ. Kinematic data from hand movements were captured using a haptic robot (*Haptic Master MK2*, Moog, Nieuw-Vennep, The Netherlands) at a sampling frequency of 400 Hz. EEG data were acquired using the BrainVision Recorder (v1.26.0001). Preprocessing and ERP analysis were performed with MNE-Python v1.8.0 [26]. For machine learning, we employed the scikit-learn library v1.5.2 [27], and statistical analyses were performed using R v4.3.3 with the lme4 v1.1-37 and lmerTest v3.1-3 packages for linear mixed models with Satterthwaite degrees of freedom approximation.

D. EEG Data Preprocessing

EEG data were first bandpass filtered using a zero-phase FIR filter (0.1–30 Hz), and a common average reference was applied. Independent Component Analysis was performed using the infomax algorithm (maximum 500 iterations) to decompose the signals. Independent components identified as muscular or ocular with a probability exceeding 0.9 were automatically detected and removed using ICLabel. All subsequent ERP and classification analyses were performed on these preprocessed data.

E. Behavioral Analyses

For all statistical analyses, we used an α level of 0.05. Due to a code error in kinematic data saving, analyses involving movement kinematics (*Trial Duration* and *Correction Onset Time*) included 12 participants ($n = 12$), while all other analyses retained the full sample ($n = 16$). We analyzed three behavioral measures: *Trial Duration* (movement onset to completion), *Hit Rate* (the proportion of successful target hits), and *Correction Onset Time*. To determine *Correction*

Onset Time, we first interpolated each trial's cursor velocity data in the x-direction (v_x) onto a uniform time grid. These interpolated velocity profiles were then averaged across trials for each participant and condition. The resulting mean velocity profile was smoothed using a Savitzky–Golay filter (window length = 15 samples, polynomial order = 2). The onset time was identified by applying a two-phase piecewise linear regression to this smoothed velocity profile, finding the optimal breakpoint within a 0–300 ms window post-movement onset. The statistical models were chosen based on the nature of the dependent variable. For the continuous measures of *Trial Duration* and *Correction Onset Time*, we employed linear mixed models (LMMs). To analyze the binary trial outcomes, *Hit Rate* was modeled using a Generalized Linear Mixed Model (GLMM) with a binomial family. For all models, we included fixed effects for trial type (Normal vs. Rotation) and experimental block (1, 2, and 3), as well as their interaction term. To account for repeated measures and inter-subject variability, subject was included as a random intercept.

F. Event-Related Potential Analysis

Epochs were extracted from −200 to 1000 ms relative to event onset (movement onset for execution errors, feedback onset for outcome errors) and were baseline-corrected using the 200 ms pre-event window. The analysis focused on two error types at the FCz (frontal) and Pz (parietal) electrodes: execution errors (Rotation vs. Normal trials) and outcome errors (Target Miss vs. Target Hit). Individual ERP waveforms were computed by averaging within-subject trials for each condition. For each participant, difference waves were computed by subtracting the averaged ERP of the correct condition from the error condition for both error types, following the standard calculation [28]:

$$\Delta\text{ERP} = \text{ERP}_{\text{error}} - \text{ERP}_{\text{correct}} \tag{2}$$

Given the challenges in defining *a priori* analysis windows in visuomotor rotation tasks [23], we employed a mass univariate approach using permutation-based dependent t-tests (10,000 permutations) across the 0–500 ms post-event window. P-values were corrected for multiple comparisons using the False Discovery Rate (FDR) [29]. Component latencies were estimated using a jackknife approach with leave-one-out averages. For identified components, mean amplitudes were extracted from 50 ms windows centered on their respective peaks. The FRN was analyzed separately in a predefined 200–400 ms window, consistent with the standard literature. These extracted amplitudes were then analyzed using an LMM.

G. EEG Classification Analysis

Two primary classification analyses were conducted: (1) Within-Block Analysis, comparing error conditions against their respective non-error conditions and against each other, and (2) Between-Block Analysis, performing pairwise comparisons of specific error conditions between experimental blocks. The framework employed within-subject classification using Support Vector Machines (SVM) [30] with a linear kernel ($C = 5$), implemented via scikit-learn. The model was evaluated using repeated ($n = 5$) stratified 5-fold cross-validation, with accuracy as the primary metric. The analysis utilized data from a 400 ms time window post-event onset (0–400 ms), with the feature space constrained to three midline electrodes (FCz, Cz, and Pz). The preprocessing pipeline involved flattening the spatio-temporal feature matrices (epochs × channels × time points) into vectors and standardizing features using a StandardScaler. For the Within-Block analyses where class imbalance was expected (e.g., Error vs. Non-Error), the majority class was downsampled to match the minority class before training. This step was omitted for the more balanced Between-Block analyses. Statistical significance was assessed using subject-level permutation tests ($n = 100$ permutations) to establish an empirical null distribution, avoiding assumptions about a theoretical chance level [31]. For each subject, a null distribution was generated by repeatedly shuffling class labels and retraining the model. The subject-level p-value was calculated as the proportion of permuted accuracies greater than or equal to the real accuracy. At the group level, one-sample t-tests were used to compare the distribution of subject-level difference scores (real accuracy - mean permuted accuracy) against zero. The resulting p-values were adjusted for multiple comparisons using the FDR procedure.

III. Results

EEG recordings were obtained from participants ($n = 16$, 4 females, age: 26 ± 3 years) who performed a task requiring them to hit a target through a reaching arm movement within a VMR paradigm (Fig. 1A). The participants controlled the cursor using a haptic robot, while their view of their arm was obscured. The task was performed across three sequential blocks to examine the influence of low-level error detection on the FRN. In the first block, participants received sensory feedback with full visual feedback of the cursor's position throughout the entire hand movement trajectory, but without explicit feedback on task success or failure. In the second block, explicit feedback on the task's success or failure was provided, yet participants did not see the cursor's position during the movement; thus, the explicit feedback disambiguated the outcome event, as no other information was available beforehand. In the third block, sensory and explicit feedback were combined. Furthermore, three key aspects of the study are crucial to highlight: (1) the primary objective of the participants was to hit as many targets as possible; (2) the participants were informed that in some trials, the cursor's position might not accurately represent the position of their hand; and (3) the order in which participants performed the tasks was sequential from Block 1 to Block 3. Each block included low-probability (20%) unexpected, random rotations, sampled from a set of equally likely magnitudes (±20° and ±40°) and distributed across 200 experimental trials per block.

A. Behavioral Results

To characterize the timing of execution error detection and the behavioral context for subsequent neural analyses, we first examined movement kinematics and task performance across the three feedback conditions.

1) Trial Duration and Correction Timing: The analysis of *Trial Duration* using a linear mixed-effects model established a baseline of 485 ms (SE = 14 ms) for normal trials in Block 3. During *Normal Trials*, duration did not significantly differ between Block 1 and Block 3 (β = 12.0 ms, 95% CI [−21.6, 45.7], $t(55)$ = 0.70, p = 0.486) or between Block 2 and Block 3 (β = −1.2 ms, 95% CI [−34.8, 32.4], $t(55)$ = −0.07, p = 0.945). The visuomotor rotation had a powerful effect in Block 3, where *Rotation Trials* were significantly longer than *Normal Trials* (β = 148.0 ms, 95% CI [114.4, 181.7], $t(55)$ = 8.63, $p < 0.001$). To test if this rotation effect was modulated by feedback availability, the interaction terms were examined. The rotation-induced increase in trial duration was significantly smaller in *Block 2* compared to *Block 3* (β = −127.8 ms, 95% CI [−175.3, −80.2], $t(55)$ = −5.27, $p < 0.001$). This interaction was not significant for *Block 1* (β = 10.9 ms, 95% CI [−36.6, 58.5], $t(55)$ = 0.45, p = 0.654). This pattern indicates that the increase in *Trial Duration* during rotation trials was greatest in Blocks 1 and 3, where visual feedback was available to enable corrections (Fig. 1B).

A second model analyzed the *Correction Onset Time* during rotation trials in Blocks 1 and 3 to investigate the timing of the corrective actions themselves. With *Block 3* and the −40° deviation as References, the model estimated a baseline correction onset of 200 ms (SE = 8 ms). The onset time did not differ significantly between Block 1 and Block 3 (β = −2.8 ms, 95% CI [−24.5, 18.8], $t(77)$ = −0.26, p = 0.798). Furthermore, the magnitude of the angular deviation had minimal effect on these initial corrections. Compared to the −40° reference, no significant differences were found for −20° (β = −6.3 ms, $t(77)$ = −0.57, p = 0.568), 20° (β = −3.2 ms, $t(77)$ = −0.29, p = 0.775), or 40° (β = 12.2 ms, $t(77)$ = 1.10, p = 0.274). Overall, participants initiated corrective movements at a highly consistent latency, regardless of the specific perturbation or the presence of explicit outcome feedback.

2) Outcome Performance: Trial-by-trial performance was analyzed using a Generalized Linear Mixed Model, with *Block 3* and *Normal Trial* set as the reference levels for all comparisons (Fig. 1C). At baseline (*Normal Trial* in *Block 3*), subjects achieved a mean hit rate of 98.2% (SE = 0.9%). The analysis revealed two significant main effects. First, on *Normal Trials*, performance in *Block 1* did not differ from *Block 3* (β = 0.25, SE = 0.40, z = 0.62, p = 0.536), whereas removing cursor feedback in *Block 2* caused a significant performance decline (β = −2.30, SE = 0.37, z = −6.31, $p < 0.001$). Second, the visuomotor rotation produced a strong, independent impairment in *Block 3*, substantially decreasing the odds of a successful hit (β = −4.90, SE = 0.44, z = −11.03, $p < 0.001$). To determine if feedback availability modulated this rotation effect, the interaction terms were examined. A marginally significant interaction was found in *Block 2*, where the absence of cursor feedback amplified the negative impact of the rotation (β = −15.90, SE = 8.37, z = −1.90, p = 0.058). This reflects a 0% hit rate, as not a single successful hit was recorded during rotation trials in this block. In contrast, the interaction for *Block 1* was not significant (β = −0.34, SE = 0.27, z = −1.29, p = 0.196). Taken together, these results show that while the visuomotor rotation impaired performance across all blocks, the combination of the rotation with the absence of online cursor feedback in *Block 2* completely eliminated successful performance.

B. Neurophysiological Results

EEG data analysis targeted two key locations: the anterior region at the FCz electrode and the posterior region at the Pz electrode. The resulting ERPs are depicted in Figure 2. The difference waves, which show the contrast between the error and non-error conditions for both error types in all blocks, are shown in Figure 3.

1) Execution Error: To establish that participants detected execution errors when visual feedback was available, we examined ERPs time-locked to movement onset.

a) Anterior response: In response to *Rotation Trials*, distinct temporal dynamics were observed at electrode FCz. In *Block 1*, the frontocentral negativity peaked at a mean latency of 230.3 ms (SE = 6.6 ms), whereas in *Block 3* it peaked at 221.9 ms (SE = 4.3 ms) post-movement onset. This timing closely aligns with the behavioral correction onset of ∼200 ms observed in these blocks, characteristic of an N2 response. Significant ($p < 0.05$) ranges were found at the FCz electrode between 222–256 ms in *Block 1*. Similarly, differences were found between 208–246 ms in *Block 3*. In contrast, *Block 2* showed no significant ERP effects, consistent with the behavioral results (Fig. 1), as participants in this block lacked the visual feedback necessary for online error detection. The N2 was succeeded by a P3a component (Fig. 3), with activity primarily centralized at the FCz and Cz electrodes exhibiting approximately equal levels of negativity at the global minima for the N2 and maxima for the P3a responses, respectively.

N2 and P3a amplitudes at the FCz electrode were analyzed using separate LMMs. The models included fixed effects for *Condition* (*Rotation Trial* vs. *Normal Trial*) and *Experimental Block* (*Block 1*, *Block 2* vs. *Block 3*), with random intercepts for each subject. *Block 3* was set as the reference level to compare conditions with partial or no visual feedback against the full feedback condition. For the N2 component, analysis of *Normal Trials* revealed that amplitude in *Block 1* was significantly more negative than in *Block 3* (β = −1.58 μV, 95% CI [−2.67, −0.49], $t(75)$ = −2.84, p = 0.006), as was *Block 2* (β = −1.76 μV, 95% CI [−2.85, −0.67], $t(75)$ = −3.17, p = 0.002). The rotation effect in *Block 3* was significant (β = −2.14 μV, 95% CI [−3.23, −1.05], $t(75)$ = −3.85, $p < 0.001$). More importantly, interaction analysis revealed how the effect of rotation on N2 amplitude differed across blocks. The rotation-induced negativity did not differ between *Block 1* and *Block 3* (β = 0.54 μV, 95% CI [−1.00, 2.08], $t(75)$ = 0.69, p = 0.491), but was significantly smaller in *Block 2* (β = 2.42 μV, 95% CI [0.88, 3.96], $t(75)$ = 3.08, p = 0.003) compared to *Block 3*.

The P3a analysis also showed block-dependent effects. On *Normal Trials*, the P3a amplitude was significantly smaller in *Block 1* (β = −1.61 μV, 95% CI [−2.82, −0.41], $t(75)$ = −2.62, p = 0.011) and *Block 2* (β = −1.99 μV, 95% CI [−3.20, −0.79], $t(75)$ = −3.24, p = 0.002) compared to *Block 3*. The rotation effect in *Block 3* was not significant (β = 0.48 μV, 95% CI [−0.73, 1.68], $t(75)$ = 0.78, p = 0.438). For the interaction, the rotation-induced P3a did not differ between *Block 1* and

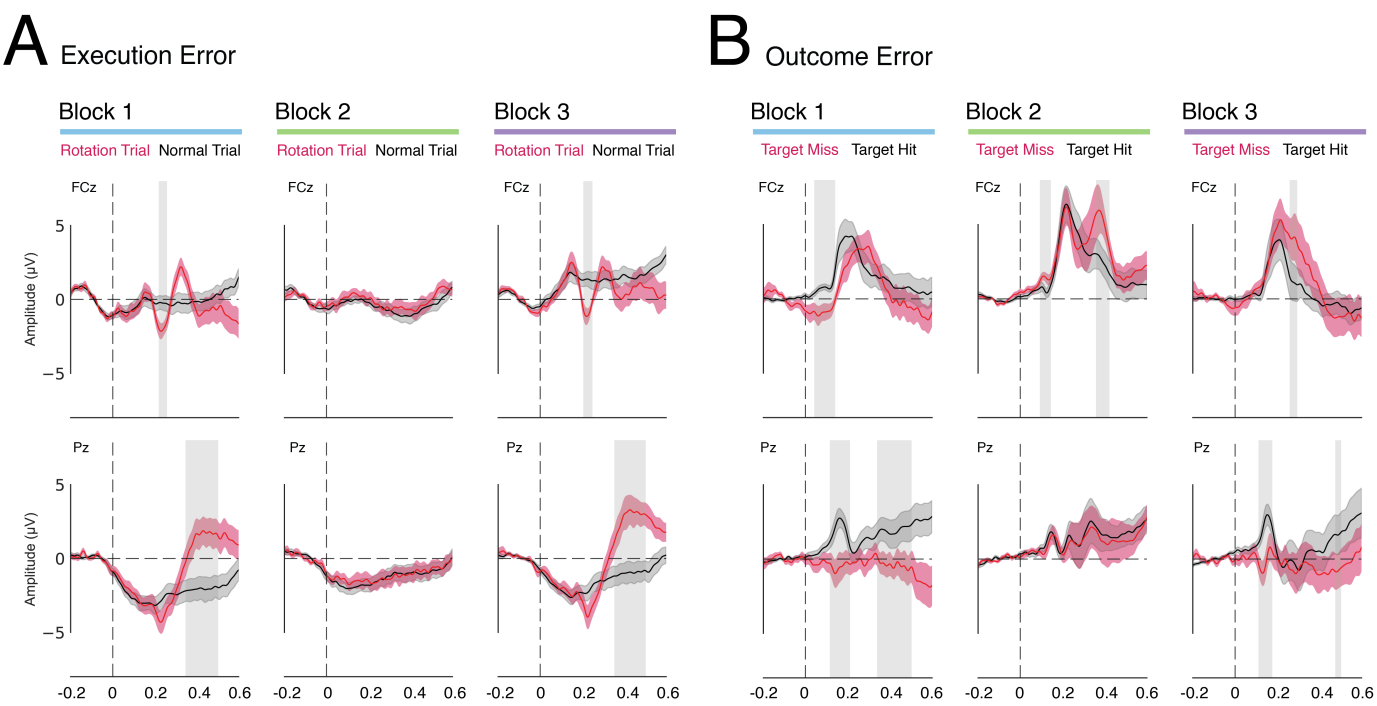

Fig. 2. **A)** Execution Error. Grand Average Condition Waves at FCz and Pz electrodes. Conditions include *Rotation Trial* and *Normal Trial*, where *Rotation Trials* cause Execution Errors. Shaded areas around the mean indicate the Standard Error of the Mean (SEM), and shaded vertical regions highlight significant differences between conditions. **B)** Outcome Error. Grand Average Condition Waves at FCz and Pz for conditions comprising *Target Miss* and *Target Hit*, with Outcome Errors resulting from Target Miss conditions. Note that due to task structure, rotation trials predominantly resulted in misses. The LMM analysis separates these effects (see Results).

Block 3 (β = 0.44 μV, 95% CI [−1.27, 2.14], $t(75)$ = 0.50, p = 0.616) or between *Block 2* and *Block 3* (β = −0.40 μV, 95% CI [−2.11, 1.30], $t(75)$ = −0.47, p = 0.643).

b) Posterior response: The posterior response at electrode Pz was characterized by a large positive deflection identified as the P3b component. In *Block 1*, this component peaked at 436.0 ms (SE = 3.9 ms). The timing was similar in *Block 3*, with the P3b peaking at 429.8 ms (SE = 15.5 ms). Mass-univariate tests identified sustained significant activity (p < 0.05) in both *Block 1* (350–500 ms) and *Block 3* (356–500 ms). To further specify the magnitude, P3b amplitudes were then analyzed using the LMM structure. The rotation effect in *Block 3* was significant (β = 4.14 μV, 95% CI [2.92, 5.37], $t(75)$ = 6.62, p < 0.001). The model's interaction analysis supported the initial findings, showing that the rotation-induced positivity did not differ between *Block 1* and *Block 3* (β = −0.34 μV, 95% CI [−2.08, 1.39], $t(75)$ = −0.39, p = 0.699), but was significantly smaller in *Block 2* (β = −4.04 μV, 95% CI [−5.77, −2.30], $t(75)$ = −4.57, p < 0.001) compared to *Block 3*.

2) Outcome Error: Having established that execution errors were detected in Blocks 1 and 3, we next examined outcome evaluation. Specifically, we tested whether FRN amplitude differed based on outcome (hit/miss) and trial type (normal/rotation).

a) Anterior response: At the FCz electrode, the feedback-related response differed notably across blocks. A canonical FRN was most clearly observed in *Block 2*, peaking at a mean latency of 262.0 ms (SE = 12.8 ms). This block's design, lacking online visual feedback, introduced ambiguity that made outcomes less predictable and feedback more salient (Fig. 1C). In contrast, the temporal dynamics in *Block 1* and *Block 3* were more variable, with evidence of earlier differential activity and less distinct FRN peaks (Fig. 2B, Fig. 3). Several analyses support these qualitative observations. Mass-univariate tests identified significant differences between *Target Miss* and *Target Hit* conditions at different times in each block: early in *Block 1* (44–138 ms), at multiple windows in *Block 2* (96–142 ms and 362–420 ms), and later in *Block 3* (262–292 ms). Further examination showed differences in latency, which was more variable in *Blocks 1* and *3* compared to the canonical pattern in *Block 2*. This latency variation might arise from component overlap with the concurrent posterior negativity observed in those blocks. Despite the early differential activity, the primary FRN response typically emerges around 200 ms post-feedback. Therefore, we conducted an LMM analysis with predictors for block, outcome (hit/miss), and trial type (normal/rotation). The model found a robust main effect of outcome in *Block 3* normal trials (β = 4.69 μV, 95% CI [2.66, 6.73], $t(142)$ = 4.52, p < 0.001), with misses eliciting more positive amplitude than hits. This outcome effect was significantly modulated by trial type (β = −3.72 μV, 95% CI [−6.63, −0.81], $t(142)$ = −2.51, p = 0.013), indicating that the FRN difference between misses and hits was smaller on rotation trials. Block interactions showed that the outcome effect was smaller in *Block 1* (β = −3.68 μV, $t(142)$ = −2.45, p = 0.015) and *Block 2* (β = −4.77 μV, $t(142)$ = −3.27, p = 0.001) compared to *Block 3*.

b) Posterior response: In addition to the anterior responses, feedback elicited a prominent posterior response at the Pz electrode that was strongly modulated by the experimental block. In *Blocks 1* and *3*, where online visual feedback was

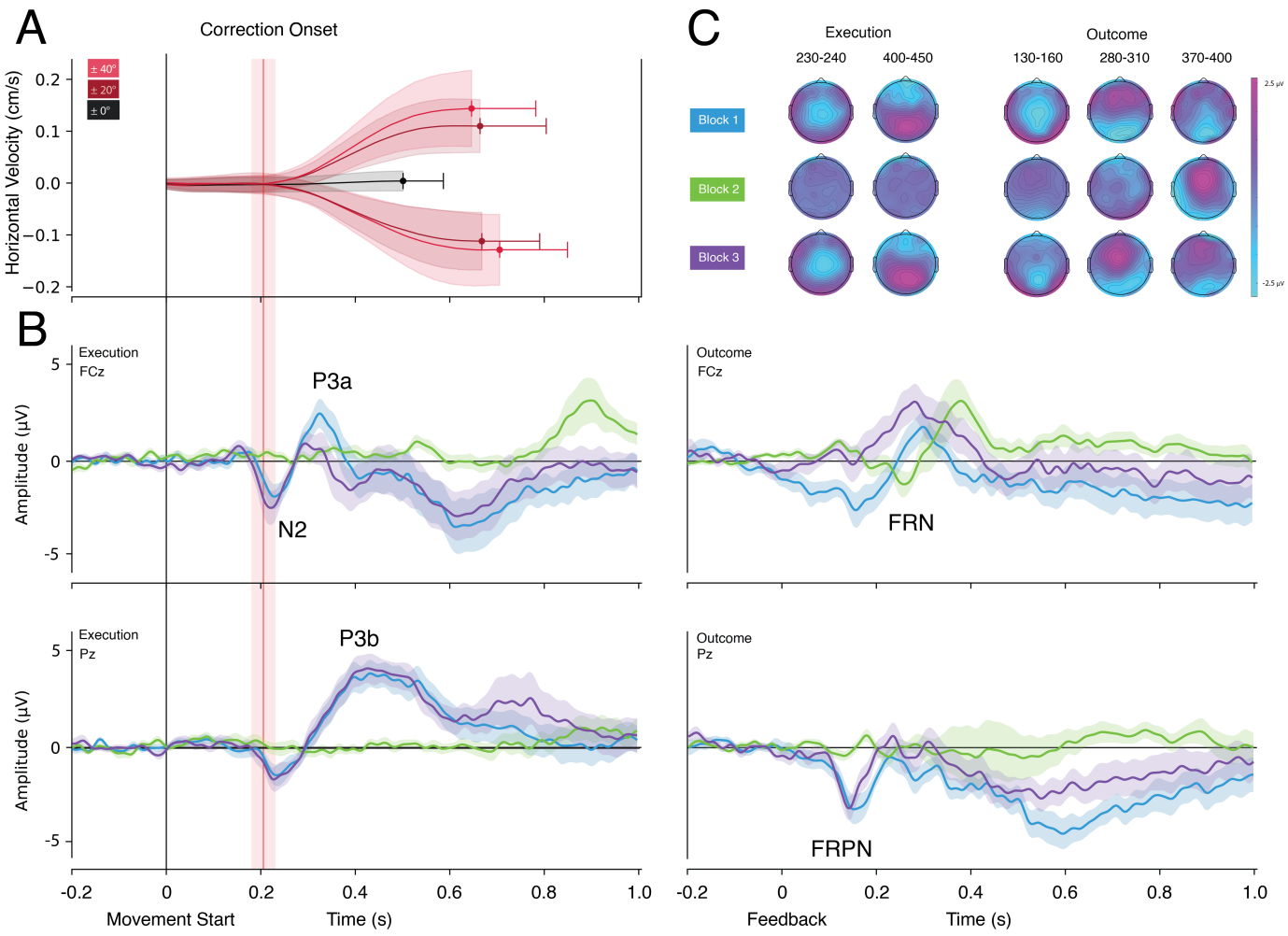

Fig. 3. **A)** Grand average horizontal velocity profile for trials in *Block 1*. The vertical dashed line and shaded region depict the mean ± SD of the *correction onset time*. **B)** Comparison of difference waves for Execution and Outcome Errors. Left: Execution Error waveforms (Rotation–Normal trials) time-locked to movement onset. Right: Outcome Error waveforms (Target Miss–Target Hit trials) time-locked to feedback. In *Blocks 2* and *3*, feedback is indicated by target color. The waveforms show distinct error-related components, including the N2, P3a, and P3b for Execution Errors and the FRN (FCz) and FRPN (Pz) for Outcome Errors. **C)** Topographical scalp distribution of the key difference wave components.

available, rotation trials produced a distinct early negative deflection at posterior electrodes relative to normal trials. We term this component the Feedback-Related Posterior Negativity (FRPN). In sharp contrast, this effect was absent in *Block 2*, where both trial types elicited a P3b-like positivity instead (Fig. 2B). Mass-univariate tests confirmed the presence of the FRPN in the feedback blocks, identifying significant time windows of 118–208 ms in *Block 1* and 114–174 ms in *Block 3*. The negativity peaked at 153.5 ms (SE = 6.4 ms) in Block 1 and 140.3 ms (SE = 2.6 ms) in Block 3. Topographically, this negativity was most prominent at Pz in Block 3, while being slightly more centralized in Block 1. Both blocks also showed additional, later periods of significant differentiation (342–500 ms in *Block 1* and 478–500 ms in *Block 3*).

An LMM analysis with predictors for block, outcome, and trial type revealed that the FRPN was not driven by outcome valence. The amplitude difference between *Target Miss* and *Target Hit* in *Block 3* normal trials was not significant ($\beta = -0.47\ \mu$V, 95% CI [−2.15, 1.21], $t(142) = -0.55$, $p = 0.584$). However, there was a significant main effect of trial type ($\beta = -2.79\ \mu$V, 95% CI [−4.50, −1.08], $t(142) = -3.20$, $p = 0.002$), indicating that rotation trials, regardless of outcome, elicited more negative posterior amplitudes than normal trials. This trial type effect was modulated by block, present in *Block 3* but significantly reduced in *Block 2* ($\beta = 2.77\ \mu$V, $t(142) = 2.31$, $p = 0.022$), where online visual feedback was unavailable. Notably, there was no outcome × trial type interaction ($\beta = 0.11\ \mu$V, $t(142) = 0.09$, $p = 0.929$), confirming that the FRPN indexes trial type (rotation vs normal) rather than outcome valence. This reframes the FRPN as reflecting feedback processing in the context of motor correction availability, rather than a pure outcome error signal.

C. Classification Results

To examine whether outcome error signals maintain consistent or distinct feature representations across feedback conditions (Objective 2), we performed within-subject classification analyses.

To assess whether the two error types were distinguishable in their neural representations, we trained classifiers using

TABLE I
CLASSIFICATION RESULTS FOR WITHIN- AND BETWEEN-BLOCK COMPARISONS

A. Within-Block Comparisons					
Block	**Event**	**Accur. (%)**	**T (df=15)**	**Cohen's d**	***p*-value**
1	Exe	65.1 ± 10.6	5.5	1.4	$p < 0.001*$
1	Out	68.0 ± 9.6	7.6	1.9	$p < 0.001*$
1	Exe vs Out	78.7 ± 10.6	9.4	2.3	$p < 0.001*$
2	Exe	50.3 ± 5.3	0.1	0.0	$p = 0.935$
2	Out	62.8 ± 8.1	6.2	1.6	$p < 0.001*$
2	Exe vs Out	82.3 ± 7.7	15.3	3.8	$p < 0.001*$
3	Exe	67.4 ± 10.0	6.8	1.7	$p < 0.001*$
3	Out	70.2 ± 8.2	9.8	2.5	$p < 0.001*$
3	Exe vs Out	83.5 ± 7.8	17.2	4.3	$p < 0.001*$
B. Between-Block Comparisons					
Block	**Event**	**Accur. (%)**	**T (df=15)**	**Cohen's d**	***p*-value**
1 vs 2	Exe	67.4 ± 11.3	6.1	1.5	$p < 0.001*$
1 vs 2	Out	78.8 ± 7.4	13.1	3.3	$p < 0.001*$
1 vs 3	Exe	57.0 ± 8.1	3.2	0.8	$p = 0.006*$
1 vs 3	Out	64.5 ± 10.5	5.3	1.3	$p < 0.001*$
2 vs 3	Exe	69.6 ± 11.4	7.0	1.8	$p < 0.001*$
2 vs 3	Out	78.6 ± 7.3	12.4	3.1	$p < 0.001*$

Within-block analysis compares real versus permuted (chance-level) classification accuracy for *Execution Errors*, *Outcome Errors*, and their direct comparison. Between-block comparisons show changes in classification accuracy across blocks for each error type. Asterisks indicate a significant difference ($p < 0.05$).

a constrained feature space from electrodes FCz, Cz, and Pz. The analyses first compared each error type to its corresponding non-error condition, then directly contrasted the error types, and lastly, compared the neural representation of each error type across blocks. *Outcome Errors* were significantly decodable in all blocks (all $p < 0.001$; see Table I). The notably higher classification accuracies in *Block 1* and *Block 3* may be attributed to either the additional motor activity from corrective actions or the distinct posterior modulations observed in those blocks. In contrast, *Execution Errors* were significantly decodable in *Block 1* and *Block 3* ($p < 0.001$), but crucially, not in *Block 2* ($p = 0.935$). This null result serves as a key control condition, as it demonstrates the classifier's inability to distinguish between *Normal* and *Rotation Trials* when both behavioral and neural responses were effectively identical (Fig. 2, Execution Error). This confirms that significant decodability in other conditions reflects genuine neural distinctions rather than arbitrary classification patterns. Furthermore, the direct classification accuracy for distinguishing between error types remained consistent across blocks. In *Block 2*, where *Execution Errors* were neurally indistinct from correct trials, this classification effectively compared *Normal Trial* and *Target Miss* conditions, yielding comparable accuracy levels.

A final comparison of the neural representations for each error type across the experimental blocks revealed distinct, block-dependent patterns. For *Outcome Errors*, comparisons showed strong differences between Blocks 1 and 2 ($p < 0.001$, $d = 3.27$) and between Blocks 2 and 3 ($p < 0.001$, $d = 3.10$), with a more moderate difference between Blocks 1 and 3 ($p < 0.001$, $d = 1.32$). *Execution Errors* showed a similar pattern, though with relatively smaller effect sizes (Block 1 vs 2: $p < 0.001$, $d = 1.52$; Block 2 vs 3: $p < 0.001$, $d = 1.75$; Block 1 vs 3: $p = 0.006$, $d = 0.81$). Overall, these results indicate a block-dependent neural pattern for both error types, where *Blocks 1* and *3* display similar characteristics in their feature space, distinctly different from the response patterns observed in *Block 2*.

IV. DISCUSSION

In a visuomotor rotation paradigm, we examined how neural correlates of low-level error detection and online correction interact with those related to high-level outcome evaluation by manipulating visual feedback availability. Our findings reveal distinct neural dynamics governing these hierarchical stages. Critically, a posterior negativity emerged during outcome processing only when visual feedback was available (*Block 1* and *Block 3*), allowing for online error detection and correction. Analysis confirmed this posterior response was not driven by outcome valence (success vs. failure), but rather by the interplay between feedback availability and the need for corrective action imposed by *Rotation trials*. Concurrently, the anterior and posterior outcome responses revealed complementary dependencies on execution context. Regarding Objective 1, the FRN differentiated misses from hits in *Blocks 1* and *3*, with reduced outcome sensitivity on rotation trials. *Block 2* showed no outcome differentiation despite a pronounced frontocentral negativity, consistent with a surprise-driven rather than valence-driven response [14] when outcome predictions cannot be formed without visual feedback. The FRPN was insensitive to outcome but strongly modulated by trial type, with rotation trials eliciting more negative amplitudes. This effect depended on visual feedback availability and was effectively absent in *Block 2*. These distinct neural signatures enabled robust classification between error types and between outcome signals arising under different feedback conditions.

The transition from low-level errors to outcome resolution revealed distinct patterns of feedback-related activity across the experimental blocks, particularly in the expression of the FRN. These results cannot be explained by a simple distinction between implicit and explicit feedback. This is evidenced by two key observations: first, neural responses in Block 1 (implicit) and Block 3 (explicit) were remarkably similar. Second, responses in Block 2 and Block 3 were distinct, despite both featuring explicit feedback. This complexity is mirrored in the posterior scalp region. In Block 1 and Block 3, we observed a Feedback-Related Posterior Negativity (FRPN) at the Pz electrode, occurring rapidly around 154 ms and 140 ms, respectively. The spatial distribution of this component implicates the parietal reach region, which is critical for representing reach goals and online motor correction [24], [32], [33], [34], [35]. Conversely, Block 2 was uniquely characterized by a prominent P3b response for both hits and misses, corroborating findings under similar conditions [19]. While these posterior systems echo those first documented by Krigolson and Holroyd [18], our findings question the proposed top-down teaching signal mechanism. The FRPN's presence depended on the block condition but was not significantly modulated by outcome valence (Target Hit vs. Miss). It remains unclear, however, whether the FRPN's dependence on block condition relates more to low-level error detection

or to the execution of corrective actions enabled by visual feedback.

Based on these findings, we interpret the FRPN as a phenomenon intrinsically linked to the processes of error detection and corrective action during the execution phase. Three primary error-related signals were identified for the execution errors: N2, P3a, and P3b. The frontocentral N2 likely reflects conflict monitoring processes, emerging when participants must override their ongoing (straight) reaching response to accommodate the rotated feedback and initiate motor reprogramming, a combined condition that creates a high degree of response conflict [36], [37]. Our analysis revealed that corrective action onset closely corresponded with the peak N2 response. While corrective actions generate additional motor activity that could potentially confound our interpretation, the consistency of our findings with studies that specifically controlled for motor-related confounds [21] supports an error-related interpretation of these signals. Following N2, we observed both the anterior P3a and the posterior P3b. The P3a response reflects novelty detection [38]. All three components showed similar patterns in *Block 1* and *Block 3* relative to *Block 2*. In *Blocks 1* and *3*, the N2 and P3b showed significant rotation effects, while the P3a showed a similar but non-significant positive trend. The parietal P3b, consistently reported in VMR paradigms [23], [39], emerges after movement correction onset, similar to Krigolson et al. [40] report in response to unexpected target jumps. Both the P3a and the P3b reflect an orienting reflex that mobilizes attentional resources for adaptation [41]. This reflex also engages the autonomic nervous system, as evidenced by changes in heart rate [42], [43] and skin conductivity [44]. Studies have shown that incorporating such autonomic measures into classifiers can improve error detection [45], suggesting additional features for error processing classification.

Our kinematic data revealed a temporal gap between movement onset and corrective actions, suggesting that error detection occurs within this interval. Whereas the ERN typically occurs 100 ms post-response [3], this timing framework does not directly apply to our paradigm, where synchronization begins at movement onset during a continuous response rather than a discrete action. Although the ERN is well-characterized for discrete responses like button presses, we propose that the early negativity in continuous movements better represents an N2 component. Previous studies have labeled similar responses ERN-Kinematic [21] or ERN [46], but the N2 framework better accounts for these findings, which may be sensitive to the magnitude of the kinematic error as reported by both studies [21], [46]. Our findings of frontocentral negativity (FCz, Cz minima) during kinematic deviation align with these studies, as well as Spüler et al.'s [10] report on execution errors. Previous research has interpreted execution errors in different ways. Krigolson and colleagues defined execution errors as situations involving an "unexpected target jump" [17]. On the other hand, Diedrichsen et al. [24] categorized reach errors into two distinct types: target errors, which occur due to unpredictable changes in the target's location (i.e., target jumps), and execution errors, which stem from failures of internal sensorimotor models. These internal models predict sensory consequences of motor commands (forward models) and compute commands to achieve goals (inverse models) [22]. Visuomotor rotation disrupts forward model predictions by altering the relationship between motor commands and visual feedback. The parietal cortex and cerebellum adapt these internal models [24]. Building on these perspectives, we suggest using the terms *Execution* and *Outcome errors* to describe distinct phases of error processing at a behavioral level. This framework acknowledges that both execution and outcome phases may encompass multiple types of error responses with distinct mechanistic origins. A critical distinction emerges between discrete and continuous action spaces during execution errors: discrete erroneous actions, such as button presses, elicit an ERN, while continuous movements evoke a similar frontocentral negativity, which we propose is better characterized as an N2 response.

The fixed block order means order effects cannot be fully excluded. However, behavioral performance and execution-phase neural responses (N2, P3b) were equivalent between Blocks 1 and 3, while Block 2 differed markedly from both, supporting feedback condition rather than order as the primary driver. The FRN outcome effect was larger in Block 3 than Block 1, which could reflect order effects or the addition of explicit outcome feedback in Block 3. Separately, rotation trials showed reduced FRN outcome sensitivity, but because these trials also involve corrective movements, longer durations, and different motor demands, we cannot attribute this reduction specifically to error detection.

Regarding Objective 2, our findings show that distinct neural patterns during outcome processing can be reliably classified. Whereas previous work [4], [10] demonstrated that execution and outcome errors produce distinguishable neural signals, our research reveals additional classification opportunities within high-level errors themselves. Specifically, we achieved mean accuracies of up to 79% when differentiating outcome errors between blocks with visual feedback (*Block 1* or *Block 3*) versus blocks without visual feedback (*Block 2*). Despite increasing task complexity, our mean classification accuracies (60–70%) align with those reported by Spüler et al. [10], varying based on the specific parameters used. In general, this approach offers the potential to generate more informative feedback signals. Detecting low-level errors can signal immediate corrective needs, while identifying high-level errors can enable broader algorithm adaptations through policy updates. The hierarchical nature of goal-directed actions, from *response* execution through *online control* to final *feedback* evaluation, produces distinct and distinguishable neural signatures. Their sequential nature suggests potential for proactive control schemes by providing predictive insights. Our findings extend the research showing that outcome information is encoded in the FRN [15], [19], with reduced outcome sensitivity on rotation trials. The FRPN complements this by indexing execution context rather than outcome valence. Together, these complementary neural manifestations provide uniquely identifiable representations of different outcome states suitable for adaptive BMI applications.

ACKNOWLEDGMENT

None of the authors have a conflict of interest to disclose.

REFERENCES

[1] M. Ullsperger, C. Danielmeier, and G. Jocham, "Neurophysiology of performance monitoring and adaptive behavior," *Physiolog. Rev.*, vol. 94, no. 1, pp. 35–79, Jan. 2014.

[2] M. Ullsperger, "Neural Bases of Performance Monitoring," in *The Wiley Handbook of Cognitive Control*. Hoboken, NJ, USA: Wiley, 2017, pp. 292–313.

[3] Z. Fu, A. Sajad, S. P. Errington, J. D. Schall, and U. Rutishauser, "Neurophysiological mechanisms of error monitoring in human and non-human primates," *Nature Rev. Neurosci.*, vol. 24, no. 3, pp. 153–172, Mar. 2023.

[4] T. Milekovic, T. Ball, A. Schulze-Bonhage, A. Aertsen, and C. Mehring, "Detection of error related neuronal responses recorded by electrocorticography in humans during continuous movements," *PLoS ONE*, vol. 8, no. 2, Feb. 2013, Art. no. e55235.

[5] Z. Fu et al., "Single-neuron correlates of error monitoring and post-error adjustments in human medial frontal cortex," *Neuron*, vol. 101, no. 1, pp. 165–177, Jan. 2019.

[6] R. Chavarriaga, A. Sobolewski, and J. D. R. Millán, "Errare machinale est: The use of error-related potentials in brain-machine interfaces," *Frontiers Neurosci.*, vol. 8, Jul. 2014, Art. no. 208.

[7] A. Kumar, L. Gao, E. Pirogova, and Q. Fang, "A review of error-related potential-based brain–computer interfaces for motor impaired people," *IEEE Access*, vol. 7, pp. 142451–142466, 2019.

[8] A. Llera, M. A. J. van Gerven, V. Gómez, O. Jensen, and H. J. Kappen, "On the use of interaction error potentials for adaptive brain computer interfaces," *Neural Netw.*, vol. 24, no. 10, pp. 1120–1127, Dec. 2011.

[9] I. Batzianoulis et al., "Customizing skills for assistive robotic manipulators, an inverse reinforcement learning approach with error-related potentials," *Commun. Biol.*, vol. 4, no. 1, pp. 1–14, Dec. 2021.

[10] M. Spüler and C. Niethammer, "Error-related potentials during continuous feedback: Using EEG to detect errors of different type and severity," *Frontiers Hum. Neurosci.*, vol. 9, p. 155, Mar. 2015.

[11] T. O. J. Gruendler, M. Ullsperger, and R. J. Huster, "Event-related potential correlates of performance-monitoring in a lateralized time-estimation task," *PLoS ONE*, vol. 6, no. 10, Oct. 2011, Art. no. e25591.

[12] S. Nieuwenhuis, C. B. Holroyd, N. Mol, and M. G. H. Coles, "Reinforcement-related brain potentials from medial frontal cortex: Origins and functional significance," *Neurosci. Biobehavioral Rev.*, vol. 28, no. 4, pp. 441–448, Jul. 2004.

[13] T. U. Hauser et al., "The feedback-related negativity (FRN) revisited: New insights into the localization, meaning and network organization," *NeuroImage*, vol. 84, pp. 159–168, Jan. 2014.

[14] F. T. P. Oliveira, J. J. McDonald, and D. Goodman, "Performance monitoring in the anterior cingulate is not all error related: Expectancy deviation and the representation of action-outcome associations," *J. Cognit. Neurosci.*, vol. 19, no. 12, pp. 1994–2004, Dec. 2007.

[15] F. Kirsch, H. Kirschner, A. G. Fischer, T. A. Klein, and M. Ullsperger, "Disentangling performance-monitoring signals encoded in feedback-related EEG dynamics," *NeuroImage*, vol. 257, Aug. 2022, Art. no. 119322.

[16] C. B. Holroyd and M. G. H. Coles, "The neural basis of human error processing: Reinforcement learning, dopamine, and the error-related negativity," *Psychol. Rev.*, vol. 109, no. 4, pp. 679–709, Oct. 2002.

[17] O. E. Krigolson and C. B. Holroyd, "Hierarchical error processing: Different errors, different systems," *Brain Res.*, vol. 1155, pp. 70–80, Jun. 2007.

[18] O. E. Krigolson and C. B. Holroyd, "Evidence for hierarchical error processing in the human brain," *Neuroscience*, vol. 137, no. 1, pp. 13–17, 2006.

[19] F. Mushtaq et al., "Distinct neural signatures of outcome monitoring after selection and execution errors," *J. Cognit. Neurosci.*, vol. 34, no. 5, pp. 748–765, Mar. 2022.

[20] D. J. Palidis, J. G. A. Cashaback, and P. L. Gribble, "Neural signatures of reward and sensory error feedback processing in motor learning," *J. Neurophysiol.*, vol. 121, no. 4, pp. 1561–1574, Apr. 2019.

[21] F. Torrecillos, P. Albouy, T. Brochier, and N. Malfait, "Does the processing of sensory and reward-prediction errors involve common neural resources? Evidence from a frontocentral negative potential modulated by movement execution errors," *J. Neurosci.*, vol. 34, no. 14, pp. 4845–4856, Apr. 2014.

[22] J. Izawa and R. Shadmehr, "Learning from sensory and reward prediction errors during motor adaptation," *PLoS Comput. Biol.*, vol. 7, no. 3, Mar. 2011, Art. no. e1002012.

[23] M. Benyamini, I. Demchenko, and M. Zacksenhouse, "Error related EEG potentials evoked by visuo-motor rotations," *Brain Res.*, vol. 1769, Oct. 2021, Art. no. 147606.

[24] J. Diedrichsen, Y. Hashambhoy, T. Rane, and R. Shadmehr, "Neural correlates of reach errors," *J. Neurosci.*, vol. 25, no. 43, pp. 9919–9931, Oct. 2005.

[25] H. Jasper, "Report of the committee on methods of clinical examination in electroencephalography," *Electroencephalogr. Clin. Neurophysiol.*, vol. 10, no. 2, pp. 370–375, May 1958.

[26] A. Gramfort et al., "MEG and EEG data analysis with MNE-Python," *Frontiers Neurosci.*, vol. 7, Dec. 2013, Art. no. 267.

[27] F. Pedregosa et al., "Scikit-learn: Machine learning in Python," *J. Mach. Learn. Res.*, vol. 12, no. 85, pp. 2825–2830, 2011.

[28] M. Falkenstein, J. Hohnsbein, J. Hoormann, and L. Blanke, "Effects of crossmodal divided attention on late ERP components. II. Error processing in choice reaction tasks," *Electroencephalogr. Clin. Neurophysiol.*, vol. 78, no. 6, pp. 447–455, Jun. 1991.

[29] Y. Benjamini and Y. Hochberg, "Controlling the false discovery rate: A practical and powerful approach to multiple testing," *J. Roy. Stat. Soc. Ser. B, Stat. Methodol.*, vol. 57, no. 1, pp. 289–300, Jan. 1995.

[30] B. E. Boser, I. M. Guyon, and V. N. Vapnik, "A training algorithm for optimal margin classifiers," in *Proc. 5th Annu. Workshop Comput. Learn. Theory*. New York, NY, USA: Association for Computing Machinery, Jul. 1992, pp. 144–152.

[31] E. Combrisson and K. Jerbi, "Exceeding chance level by chance: The caveat of theoretical chance levels in brain signal classification and statistical assessment of decoding accuracy," *J. Neurosci. Methods*, vol. 250, pp. 126–136, Jul. 2015.

[32] D. Baldauf, H. Cui, and R. A. Andersen, "The posterior parietal cortex encodes in parallel both goals for double-reach sequences," *J. Neurosci.*, vol. 28, no. 40, pp. 10081–10089, Oct. 2008.

[33] G. H. Mulliken, S. Musallam, and R. A. Andersen, "Decoding trajectories from posterior parietal cortex ensembles," *J. Neurosci.*, vol. 28, no. 48, pp. 12913–12926, Nov. 2008.

[34] R. Breveglieri et al., "RTMS over the human medial parietal cortex impairs online reaching corrections," *Brain Struct. Function*, vol. 229, no. 2, pp. 297–310, Dec. 2023.

[35] F. Filimon, J. D. Nelson, R.-S. Huang, and M. I. Sereno, "Multiple parietal reach regions in humans: Cortical representations for visual and proprioceptive feedback during on-line reaching," *J. Neurosci.*, vol. 29, no. 9, pp. 2961–2971, Mar. 2009.

[36] J. R. Folstein and C. Van Petten, "Influence of cognitive control and mismatch on the N2 component of the ERP: A review," *Psychophysiology*, vol. 45, no. 1, pp. 152–170, Jan. 2008.

[37] M. M. Botvinick, J. D. Cohen, and C. S. Carter, "Conflict monitoring and anterior cingulate cortex: An update," *Trends Cognit. Sci.*, vol. 8, no. 12, pp. 539–546, Dec. 2004.

[38] J. Polich, "Updating p300: An integrative theory of P3a and P3b," *Clin. Neurophysiol.*, vol. 118, no. 10, pp. 2128–2148, Oct. 2007.

[39] S. J. MacLean, C. D. Hassall, Y. Ishigami, O. E. Krigolson, and G. A. Eskes, "Using brain potentials to understand prism adaptation: The error-related negativity and the P300," *Frontiers Hum. Neurosci.*, vol. 9, Jun. 2015, Art. no. 335.

[40] O. E. Krigolson, C. B. Holroyd, G. Van Gyn, and M. Heath, "Electroencephalographic correlates of target and outcome errors," *Exp. Brain Res.*, vol. 190, no. 4, pp. 401–411, Oct. 2008.

[41] J. R. Wessel, "An adaptive orienting theory of error processing," *Psychophysiology*, vol. 55, no. 3, Mar. 2018, Art. no. e13041.

[42] S. G. Danev and C. R. de Winter, "Heart rate deceleration after erroneous responses," *Psychologische Forschung*, vol. 35, no. 1, pp. 27–34, Mar. 1971.

[43] J. R. Wessel, C. Danielmeier, and M. Ullsperger, "Error awareness revisited: Accumulation of multimodal evidence from central and autonomic nervous systems," *J. Cognit. Neurosci.*, vol. 23, no. 10, pp. 3021–3036, Oct. 2011.

[44] G. Hajcak, N. McDonald, and R. F. Simons, "To err is autonomic: Error-related brain potentials, ANS activity, and post-error compensatory behavior," *Psychophysiology*, vol. 40, no. 6, pp. 895–903, Nov. 2003.

[45] M. Wimmer, N. Weidinger, E. Veas, and G. R. Müller-Putz, "Multimodal decoding of error processing in a virtual reality flight simulation," *Sci. Rep.*, vol. 14, no. 1, p. 9221, Apr. 2024.

[46] F. Iwane, A. Billard, and J. D. R. Millán, "Inferring individual evaluation criteria for reaching trajectories with obstacle avoidance from EEG signals," *Sci. Rep.*, vol. 13, no. 1, p. 20163, Nov. 2023.